Hindawi
Advances in Civil Engineering
Volume 2020, Article ID 8827737, 13 pages
https://doi.org/10.1155/2020/8827737

Research Article

Dynamic Stress Analysis of a Circular-Lined Tunnel in Composite Strata-SH Wave Incidence

Hui Qi, Yang Zhang, Jing Guo, and Fuqing Chu

College of Aerospace and Civil Engineering, Harbin Engineering University, Harbin 150001, China

Correspondence should be addressed to Yang Zhang; zhangyang1987@hrbeu.edu.cn

Received 12 August 2020; Revised 12 September 2020; Accepted 15 September 2020; Published 29 September 2020

Academic Editor: Mehmet Serkan Kirgiz

It is necessary to study the problem of seismic wave scattering in composite stratum for tunnel engineering because the existence of composite strata will make the stress of tunnels more complicated during earthquakes. In this thesis, a series solution of the scattering wave field of the composite strata and lining is obtained using the complex function method. According to the stress and displacement boundary conditions between the composite stratum and the lining, a series of equations are established and are solved by means of Fourier transformation and finite term truncation, and the calculation errors are also discussed. Through programming calculations, the dynamic stress concentration factor (*DSCF*) of circular tunnels in the two types of composite strata, "hard-over-soft" and "soft-over-hard," is analyzed when SH waves propagate, and certain conclusions on the scattering of SH waves that are distinguished from the case of single homogeneous layers are reached. The research in this article reveals some phenomena. For the Q345 steel lining in the calculation examples, it is found in this paper that increasing the thickness of the lining is effective to reduce the influence of the *DSCF*. But, for C30 concrete, increasing the thickness of the lining reduces the *DSCF* of the outer surface while increasing the *DSCF* of the inner surface.

1. Introduction

Urban lifeline projects such as subway tunnels, water supply and drainage pipelines, and natural gas and oil pipelines are important components of urban structures and are effective means to solve urban land shortage and relieve traffic pressure. Damage of these due to an earthquake will not only directly threaten human lives but also cause indirect hazards such as water supply interruption, fires, and epidemics. This indirect damage sometimes causes more losses than direct damage. The seismic research on tunnels and pipeline engineering is therefore an important topic of urban disaster prevention and mitigation, and it has been one of the hot issues studied by scholars from various countries [1–5].

Earthquakes are internal dynamic geological processes. Rock vibration is propagated in the form of elastic waves through the particles of the rock. The destructive consequences of earthquakes are directly or indirectly related to seismic waves. That is why the study of seismic waves has become the basic work of studying and predicting earthquakes. In nature, many strata have undergone geological actions such as crustal movement, earthquakes, metamorphism, weathering, deposition, and transportation during the long process of geological evolution, forming alternately overlapping soft and hard rock layers, which are intricately complex shapes that we often call composite strata [6]. A composite stratum is often composed of two or more strata with different physical and mechanical parameters. The most typical combinations are "soft-over-hard" and "hard-over-soft." When the composite stratum is "hard-over-soft," the stability of the lower soft soil is higher because the upper hard soil layer supports the lower soft soil. If the composite stratum is "soft-over-hard," there is often the problem of instability of the excavation surface when the upper soft soil is excavated [7, 8]. The composite strata not only bring many technical difficulties to the construction of the tunnel but also cause great difficulties in the study of seismic waves because the mechanical parameters of the composite strata are variable and the scattered wave fields of the various soil layers interfere with each other. So far, many

research results on seismic wave scattering have simplified the Earth into a single homogeneous elastic whole-space or half-space [9–14]. However, in actual engineering, the geological conditions are complex and changeable, seismic oscillation is greatly affected by the types of sites and propagation paths, and site differences have a great influence on the propagation of seismic waves of different frequencies. The research on the elastic wave scattering of tunnels lined with composite strata is therefore of important engineering significance. In addition, the material and thickness of the tunnel lining are important factors to consider in engineering design. They will significantly affect the dynamic stress distribution of the lining under earthquakes, making it necessary to conduct in-depth discussions.

During the propagation of seismic waves, when encountering the boundary of the tunnel, secondary waves will occur at the boundary, which is also called wave scattering. Meanwhile, the stress at the edge of the tunnel will suddenly change, resulting in dynamic stress concentration. Analytical methods such as wave function expansion method, integral equation method, and asymptotic matching method and numerical methods such as T matrix method, singular boundary method (SBM), and finite element method are all important methods for studying elastic wave scattering problems [15–21]. Numerical methods are advantageous tools for solving engineering problems under complex geological conditions. In recent years, Ba et al. used the indirect boundary element method (IBEM) to study the scattering problem in a multilayered half-space. This method has been applied to the study of problems in some complex terrains such as canyon, partially filled alluvial valley, fully filled alluvial valley, and layered valley-hill coupled topography, and many valuable results are produced [22–24]. However, using the analytical method to study the wave problem in the composite stratum is of great help for us to understand the physical phenomena and laws of the problem and helps us to estimate the practical problems on the order of magnitude. This thesis is based on analytical methods, focusing on the *DSCF* around the lining tunnel in the composite strata when SH waves are incident. Based on the function of complex variables (CVF), we use the big circle method to simulate the straight line boundary with the arc boundary and the coordinate translation method and Hankel series to establish the wave fields of each soil layer and the tunnel boundary, and the problem is solved in series solution [25–29]. On the basis of theoretical derivation, two typical examples—concrete and steel-lined tunnels in composite strata—are analyzed. The frequency of incident waves, soil layer and lining parameters, lining thickness, and other factors affect the dynamics of the lining.

2. Theoretical Model and Fundamental Equations

2.1. Theoretical Model. Figure 1 is the composite strata model studied in this paper. The lower soil layer is Layer A, and the surface soil layer is Layer B with the thickness being d, and the upper and the lower boundaries of Layer B are Γ_u and Γ_d. Region C is a circular-lining tunnel located in the

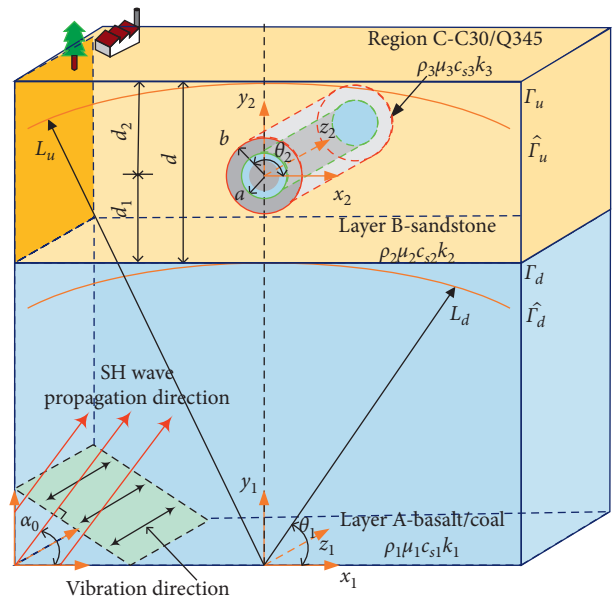

Figure 1: The composite strata model.

surface soil layer. The distance between the center O_2 and Γ_u is d_2 and the distance from Γ_d is d_1.

Draw a vertical line through the center of the lining O_2 to the depth of the lower soil layer, and take a point O_1 on the vertical line to establish the spatial overall rectangular coordinate system $X_1Y_1Z_1$, and make two arcs with O_1 as the center which are, respectively, tangent with the upper and lower boundaries of the surface soil layer. The upper boundary Γ_u of the surface soil layer becomes a circular arc $\widehat{\Gamma_u}$, and the lower boundary Γ_d becomes a circular arc $\widehat{\Gamma_d}$, and then the center of the lining is the spatial local rectangular coordinate system $X_2Y_2Z_2$. The green plane represents the wavefront of the plane SH wave. The angle between the propagation direction and X is α_0. Since the problem we study is a plane strain problem, it is simplified to a problem on the XY plane. θ_1 and θ_2 are the angle variables in the coordinate systems $X_1O_1Y_1$ and $X_2O_2Y_2$, respectively. The radius of the arc $\widehat{\Gamma_u}$ is L_u, the radius of the arc $\widehat{\Gamma_d}$ is L_d, the outer diameter of the lining is b, and the inner diameter is a.

The Earth has formed various geological forms after undergoing the evolution of various geological cycles. Sedimentary rocks are often formed by sedimentation in different periods, usually located on the surface of the Earth, and common sandstone, conglomerate, limestone, and so forth. Metamorphic rock is the transformation of rock under the influence of internal dynamic factors such as high temperature and high pressure. It is often at a certain depth below the surface. The representative ones are marble and basalt. Among them, basalt is the most widely distributed rock on Earth. Therefore, we choose sandstone and basalt, the most common stratigraphic combination in engineering, as the research object of the "soft-above-hard" stratigraphic combination in this paper. In cities with coal mines, while hard sandstone exists on the surface, there are relatively soft coal seams in the lower part, forming a "hard-over-soft" composite stratum, which is also studied in this paper.

The density, shear wave speeds, shear moduli, and SH wave numbers of the three regions in the model are represented by symbols ρ, c_S, μ, and k. Figure 2 lists the mechanical indexes of the three types of rocks and two types of lining materials related to the research in this paper. Define $c_S^* = (c_{S2}/c_{S1})$, $c_S^\# = (c_{S3}/c_{S1})$, $\rho^* = (\rho_2/\rho_1)$, $\rho^\# = (\rho_3/\rho_1)$, $k^* = (k_2/k_1)$, and $k^\# = (k_3/k_1)$; and, from $k = (\omega/c_S)$, we know $k^* = (1/c_S^*) = \sqrt{\rho^*/\mu^*}$ and $k^\# = (1/c_S^\#) = \sqrt{\rho^\#/\mu^\#}$. When $k^* > 1$, it indicates that the surface soil layer is "softer" than the lower soil layer; that is, the composite stratum is "soft-over-hard". We call it Condition A. Reversely, the composite stratum of "hard-above-soft" type is called Condition B. Similarly, it can be known from the parameters of the two lining materials that when the lining is made of Q345 steel, $(k_3/k_2) = (c_{S2}/c_{S3}) = 0.8$, indicating that the lining is "harder" than Domain II and is called "rigid lining"; when we adopt C30 concrete, $(k_3/k_2) = (c_{S2}/c_{S3}) = 1.1$, indicating that the lining is "softer" than Domain II and is called "flexible lining."

2.2. Wave Fields in Composite Strata. The CVF was introduced to depict the rectangular coordinate systems. The complex plane corresponding to the rectangular coordinate system $X_1O_1Y_1$ is $(z_1, \overline{z}_1)$, where $z_1 = x_1 + iy_1$ and $\overline{z}_1 = x_1 - iy_1$. Similarly, the complex plane corresponding to the rectangular coordinate system $X_2O_2Y_2$ is $(z_2, \overline{z}_2)$, where $z_2 = x_2 + iy_2$ and $\overline{z}_2 = x_2 - iy_2$. Besides,

$$z_1 = z_2 + (d_1 + L_d)i. \tag{1}$$

The problem deals with a steady-state SH wave; the displacement solution can be obtained by the method of separation of variables. Bring the displacement solution into the wave equation to obtain the Helmholtz equation in the complex plane $(z, \overline{z})$ as in [13]. According to the idea of "decompose" and "connect," we will break down the problem into two parts for analysis. First, we construct the scattering wave field of the circular hole problem in the composite stratum and then the standing wave field in the lining, and finally we solve the equation through the continuous boundary conditions of the two. Figure 3 shows a schematic diagram of the SH incident wave, the scattered wave fields of the boundary of each soil layer, and the scattered wave fields of a circular hole with a radius of b.

In the $(z_1, \overline{z}_1)$ plane, the plane SH incident wave satisfying the Helmholtz equation in the lower soil layer can be expressed as

$$w_1^{(i)} = w_0 \exp\left[ik_1 \mathrm{Re}\left(z_1 e^{-i\alpha_0}\right)\right]. \tag{2}$$

The corresponding radial stress is

$$\tau_{z\rho 1}^{(i)} = ik_1\mu_1 w_0 \exp\left[ik_1 \mathrm{Re}\left(z_1 e^{-i\alpha_0}\right)\right] \mathrm{Re}\left[\frac{\left(z_1 e^{-i\alpha_0}\right)}{|z_1|}\right]. \tag{3}$$

Soil layer and lining material parameters			
	Name	Density (kg/m^3)	Shear velocity (m/s)
Layer A	Basalt	3,100	4,000
	Coal	1,500	1,000
Layer B	Sandstone	2,800	2,500
Lining	C30 concrete	2,400	2,240
	Q345 steel	7,850	3 160

Figure 2: Parameters of soil layer and lining material of the composite strata model.

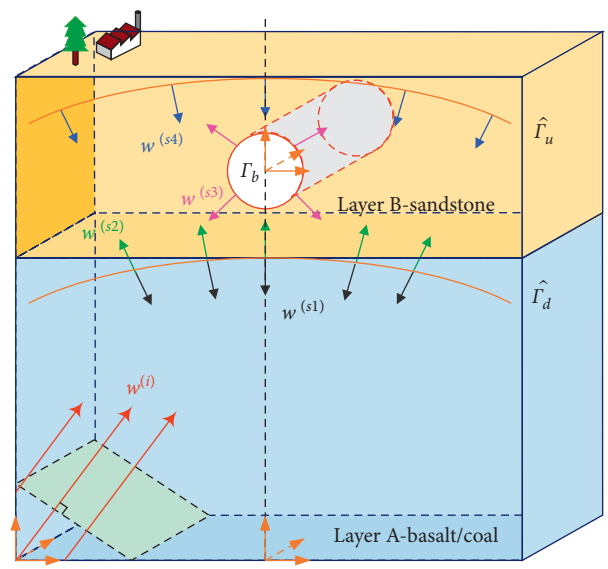

Figure 3: Scattered wave field in composite strata.

From the asymptotic nature of the Hankel wave function, it can be seen that all the scattered waves caused by the cylindrical surface spreading outward can be written as a series solution expanded by the first kind of Hankel function, and all the scattered waves converging and propagating inward can be written as a series solution expanded by the second Hankel wave function, thus constructing the form of the scattered wave in each coordinate system. Define the undetermined constants C_{An}, C_{Bn}, C_{Cn}, C_{Dn}, C_{En}, and C_{Fn}.

The waves scattered by the boundary Γ_d in lower soil layer and surface soil layer are denoted as $w_1^{(S1)}$ and $w_1^{(S2)}$, respectively

$$\begin{aligned} w_1^{(S1)} &= \sum_{n=-\infty}^{n=+\infty} C_{An} H_n^{(2)}\left[k_1 (z_1\overline{z}_1)^{1/2}\right]\left(\frac{z_1}{\overline{z}_1}\right)^{n/2}, \\ w_1^{(S2)} &= \sum_{n=-\infty}^{n=+\infty} C_{Bn} H_n^{(1)}\left[k_2 (z_1\overline{z}_1)^{1/2}\right]\left(\frac{z_1}{\overline{z}_1}\right)^{n/2}. \end{aligned} \tag{4}$$

The corresponding radial stress is

$$\tau_{z\rho 1}^{(S1)} = \frac{k_1\mu_1}{2}\sum_{n=-\infty}^{n=+\infty} C_{An}\left\{H_{n-1}^{(2)}\left[k_1\left(z_1\overline{z}_1\right)^{1/2}\right] - H_{n+1}^{(2)}\left[k_1\left(z_1\overline{z}_1\right)^{1/2}\right]\right\}\left(\frac{z_1}{\overline{z}_1}\right)^{n/2},$$
$$\tau_{z\rho 1}^{(S2)} = \frac{k_2\mu_2}{2}\sum_{n=-\infty}^{n=+\infty} C_{Bn}\left\{H_{n-1}^{(1)}\left[k_2\left(z_1\overline{z}_1\right)^{1/2}\right] - H_{n+1}^{(1)}\left[k_2\left(z_1\overline{z}_1\right)^{1/2}\right]\right\}\left(\frac{z_1}{\overline{z}_1}\right)^{n/2}. \quad (5)$$

Define the undetermined constants $\Omega^- = z_1 - i(d_1 + L_d)$ and $\Omega^+ = z_2 + i(d_1 + L_d)$.

Using the method of coordinate translation, we can express $w_1^{(S2)}$ in the complex plane $(z_2, \overline{z}_2)$ as

$$w_2^{(S2)} = \sum_{n=-\infty}^{n=+\infty} C_{Bn}H_n^{(1)}\left(k_2\left|\chi^+\right|\right)\left(\frac{\chi^+}{\left|\chi^+\right|}\right)^n,$$
$$\tau_{z\rho 2}^{(S2)} = \frac{k_2\mu_2}{2}\sum_{n=-\infty}^{n=+\infty} C_{Bn}\left\{H_{n-1}^{(1)}\left[k_2\left|\Omega^+\right|\right]\left[\frac{\Omega^+}{\left|\Omega^+\right|}\right]^{n-1}\frac{z_2}{\left|z_2\right|} - H_{n+1}^{(1)}\left[k_2\left|\Omega^+\right|\right]\left[\frac{\Omega^+}{\left|\Omega^+\right|}\right]^{n+1}\frac{\overline{z}_2}{\left|z_2\right|}\right\}. \quad (6)$$

In the $(z_2, \overline{z}_2)$ plane, the scattered wave $w_2^{(S3)}$ generated by the boundary Γ_b of the circular hole in the surface soil can be expressed as

$$w_2^{(S3)} = \sum_{n=-\infty}^{n=+\infty} C_{Cn}H_n^{(1)}\left[k_2\left(z_2\overline{z}_2\right)^{1/2}\right]\left(\frac{z_2}{\overline{z}_2}\right)^{n/2},$$
$$\tau_{z\rho 2}^{(S3)} = \frac{k_2\mu_2}{2}\sum_{n=-\infty}^{n=+\infty} C_{Cn}\left\{H_{n-1}^{(1)}\left[k_2\left(z_2\overline{z}_2\right)^{1/2}\right] - H_{n+1}^{(1)}\left[k_2\left(z_2\overline{z}_2\right)^{1/2}\right]\right\}\left(\frac{z_2}{\overline{z}_2}\right)^{n/2}. \quad (7)$$

Using the method of coordinate translation, we can express them in the complex plane $(z_1, \overline{z}_1)$ as

$$w_1^{(S3)} = \sum_{n=-\infty}^{n=+\infty} C_{Cn}H_n^{(1)}\left[k_2\left|\Omega^-\right|\right]\left[\frac{\Omega^-}{\left|\Omega^-\right|}\right]^n,$$
$$\tau_{z\rho 1}^{(S3)} = \frac{k_2\mu_2}{2}\sum_{n=-\infty}^{n=+\infty} C_{Cn}\left\{H_{n-1}^{(1)}\left[k_2\left|\Omega^-\right|\right]\left[\frac{\Omega^-}{\left|\Omega^-\right|}\right]^{n-1}\frac{z_1}{\left|z_1\right|} - H_{n+1}^{(1)}\left[k_2\left|\Omega^-\right|\right]\left[\frac{\Omega^-}{\left|\Omega^-\right|}\right]^{n+1}\frac{\overline{z}_1}{\left|z_1\right|}\right\}. \quad (8)$$

In the $(z_1, \overline{z}_1)$ plane, the scattered wave $w_1^{(S4)}$ generated by the boundary Γ_u in the surface soil layer can be expressed as

$$w_1^{(S4)} = \sum_{n=-\infty}^{n=+\infty} C_{Dn}H_n^{(2)}\left[k_2\left(z_1\overline{z}_1\right)^{1/2}\right]\left(\frac{z_1}{\overline{z}_1}\right)^{n/2},$$
$$\tau_{z\rho 1}^{(S4)} = \frac{k_1\mu_1}{2}\sum_{n=-\infty}^{n=+\infty} C_{Dn}\left\{H_{n-1}^{(2)}\left[k_2\left(z_1\overline{z}_1\right)^{1/2}\right] - H_{n+1}^{(2)}\left[k_2\left(z_1\overline{z}_1\right)^{1/2}\right]\right\}\left(\frac{z_1}{\overline{z}_1}\right)^{n/2}. \quad (9)$$

Using the method of coordinate translation, we can express them in the complex plane $(z_2, \overline{z}_2)$ as

$$w_2^{(S4)} = \sum_{n=-\infty}^{n=+\infty} C_{Dn}H_n^{(2)}\left[k_2\left|\Omega^+\right|\right]\left[\frac{\Omega^+}{\left|\Omega^+\right|}\right]^n,$$
$$\tau_{z\rho 2}^{(S4)} = \frac{k_2\mu_2}{2}\sum_{n=-\infty}^{n=+\infty} C_{Dn}\left\{H_{n-1}^{(2)}\left[k_2\left|\Omega^+\right|\right]\left[\frac{\Omega^+}{\left|\Omega^+\right|}\right]^{n-1}\frac{z_2}{\left|z_2\right|} - H_{n+1}^{(2)}\left[k_2\left|\Omega^+\right|\right]\left[\frac{\Omega^+}{\left|\Omega^+\right|}\right]^{n+1}\frac{\overline{z}_2}{\left|z_2\right|}\right\}. \quad (10)$$

The boundary conditions are as follows:

Continuous displacement on the lower boundary of the surface soil layer:

$$w_1^{(i)} + w_1^{(S1)} = w_1^{(S2)} + w_1^{(S3)} + w_1^{(S4)}\Big|_{|z_1|=L_d}. \quad (11)$$

Continuous radial stress on the lower boundary of the surface soil layer:

$$\tau_{z\rho 1}^{(i)} + \tau_{z\rho 1}^{(S1)} = \tau_{z\rho 1}^{(S2)} + \tau_{z\rho 1}^{(S3)} + \tau_{z\rho 1}^{(S4)}\Big|_{|z_1|=L_d}. \quad (12)$$

Free radial stress on the upper boundary of the surface soil layer:

$$\tau_{z\rho 1}^{(S2)} + \tau_{z\rho 1}^{(S3)} + \tau_{z\rho 1}^{(S4)} = 0\Big|_{|z_1|=L_u}. \quad (13)$$

2.3. Wave Fields in the Lining. Figure 4 shows a schematic diagram of the scattered waves inside the lining.

In the $(z_2, \overline{z}_2)$ plane, the waves scattered by the lining outer surface, Γ_b, and the inner surface, Γ_a, can be denoted as $w_2^{(\Gamma b)}$ and $w_2^{(\Gamma a)}$, respectively, and can be expressed as follows:

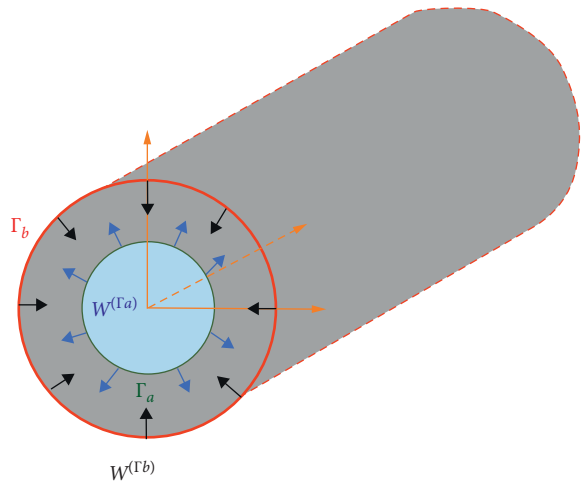

Figure 4: Scattered waves in the lining.

$$w_2^{(\Gamma b)} = \sum_{n=-\infty}^{n=+\infty} C_{En} H_n^{(2)}(k_3 b)\left(\frac{z_2}{\bar{z}_2}\right)^{n/2},$$

$$\tau_{z\rho 2}^{(\Gamma b)} = \frac{k_3\mu_3}{2}\sum_{n=-\infty}^{n=+\infty} C_{En}\left[H_{n-1}^{(2)}(k_3 b) - H_{n+1}^{(2)}(k_3 b)\right]\left(\frac{z_2}{\bar{z}_2}\right)^{n/2},$$

$$w_2^{(\Gamma a)} = \sum_{n=-\infty}^{n=+\infty} C_{Fn} H_n^{(1)}(k_3 a)\left(\frac{z_2}{\bar{z}_2}\right)^{n/2},$$

$$\tau_{z\rho 2}^{(\Gamma a)} = \frac{k_3\mu_3}{2}\sum_{n=-\infty}^{n=+\infty} C_{Fn}\left[H_{n-1}^{(1)}(k_3 a) - H_{n+1}^{(1)}(k_3 a)\right]\left(\frac{z_2}{\bar{z}_2}\right)^{n/2}. \tag{14}$$

The boundary conditions are as follows:

Continuous displacement on the outer surface of the lining:

$$w_2^{(S2)} + w_2^{(S3)} + w_2^{(S4)} = w_2^{(\Gamma b)} + w_2^{(\Gamma a)}\Big|_{|z_2|=b}. \tag{15}$$

Continuous radial stress on the outer surface of the lining:

$$\tau_{z\rho 2}^{(S2)} + \tau_{z\rho 2}^{(S3)} + \tau_{z\rho 2}^{(S4)} = \tau_{z\rho 2}^{(\Gamma b)} + \tau_{z\rho 2}^{(\Gamma a)}\Big|_{|z_2|=b}. \tag{16}$$

Free radial stress on the inner surface of the lining:

$$\tau_{z\rho 2}^{(\Gamma b)} + \tau_{z\rho 2}^{(\Gamma a)} = 0\big|_{|z_2|=a}. \tag{17}$$

3. Equation Solving and Error Analysis

Transform the boundary condition expression:

$$\begin{cases} w_1^{(S1)} - w_1^{(S2)} - w_1^{(S3)} - w_1^{(S4)} = -w_1^{(i)}, & |z_1| = L_d, \\ \tau_{z\rho 1}^{(S1)} - \tau_{z\rho 1}^{(S2)} - \tau_{z\rho 1}^{(S3)} - \tau_{z\rho 1}^{(S4)} = -\tau_{z\rho 1}^{(i)}, & |z_1| = L_d, \\ \tau_{z\rho 1}^{(S2)} + \tau_{z\rho 1}^{(S3)} + \tau_{z\rho 1}^{(S4)} = 0, & |z_1| = L_u, \\ w_2^{(S2)} + w_2^{(S3)} + w_2^{(S4)} - w_2^{(\Gamma b)} - w_2^{(\Gamma a)} = 0, & |z_2| = b, \\ \tau_{z\rho 2}^{(S2)} + \tau_{z\rho 2}^{(S3)} + \tau_{z\rho 2}^{(S4)} - \tau_{z\rho 2}^{(\Gamma b)} - \tau_{z\rho 2}^{(\Gamma a)} = 0, & |z_2| = b, \\ \tau_{z\rho 2}^{(\Gamma b)} + \tau_{z\rho 2}^{(\Gamma a)} = 0, & |z_2| = a. \end{cases} \tag{18}$$

By Fourier series at both ends of the angle variable θ, an infinite set of equations with infinite unknown coefficients will be obtained:

$$\sum_{m=-\infty}^{m=+\infty}\sum_{n=-\infty}^{n=+\infty}\begin{bmatrix} +\zeta_{mn}^{(11)} & -\zeta_{mn}^{(12)} & -\zeta_{mn}^{(13)} & -\zeta_{mn}^{(14)} & 0 & 0 \\ +\zeta_{mn}^{(21)} & -\zeta_{mn}^{(22)} & -\zeta_{mn}^{(23)} & -\zeta_{mn}^{(24)} & 0 & 0 \\ 0 & +\zeta_{mn}^{(32)} & +\zeta_{mn}^{(33)} & +\zeta_{mn}^{(34)} & 0 & 0 \\ 0 & +\zeta_{mn}^{(42)} & +\zeta_{mn}^{(43)} & +\zeta_{mn}^{(44)} & -\zeta_{mn}^{(45)} & -\zeta_{mn}^{(46)} \\ 0 & +\zeta_{mn}^{(52)} & +\zeta_{mn}^{(53)} & +\zeta_{mn}^{(54)} & -\zeta_{mn}^{(55)} & -\zeta_{mn}^{(56)} \\ 0 & 0 & 0 & 0 & +\zeta_{mn}^{(65)} & +\zeta_{mn}^{(66)} \end{bmatrix} \cdot \begin{bmatrix} C_{An} \\ C_{Bn} \\ C_{Cn} \\ C_{Dn} \\ C_{En} \\ C_{Fn} \end{bmatrix} = \sum_{m=-\infty}^{m=+\infty}\begin{bmatrix} -\eta_m^1 \\ -\eta_m^2 \\ 0 \\ 0 \\ 0 \\ 0 \end{bmatrix}. \tag{19}$$

According to the attenuation properties of the Hankel function, the finite terms of m and n can be intercepted under the condition of ensuring accuracy, the above equations can be transformed into finite linear equations, and the undetermined constants can be obtained.

The main purpose of the numerical programming calculation is to analyze the dynamic stress concentration phenomenon around the lining in the model of this paper. We will make the media parameters dimensionless and also use the dimensionless results in the analysis of the results. Assume the parameters of Domain I: $\rho_1 = 1$, $c_{S1} = 1$, and $k_1 = 1$; and the shear modulus $\mu_1 = 1$ can be obtained from $c_S = (\sqrt{\mu/\rho})$. Figure 5 shows the values of the composite stratum and the lining after dimensionless conversion.

The calculation error mainly comes from two aspects. The first source of error is the error caused by truncating the Fourier-Hankel wave function series and truncating infinite linear algebraic equations into finite linear algebraic

Dimensionless parameter values					
Assume layer A : $\rho_1 = 1, \mu = 1, c_{s1} = 1, k_1 = 1$					
	ρ^*	k^*	Lining	$\rho^\#$	$k^\#$
Condition A basalt + sandstone	0.90	1.60	C30 concrete	0.77	1.80
			Q345 steel	2.53	1.27
Condition B coal + sandstone	1.87	0.40	C30 concrete	1.60	0.45
			Q345 steel	5.20	0.30

Figure 5: Dimensionless parameters of composite strata and linings.

equations. The second source of error lies in the fact that the large-arc assumption method is an approximation method. In fact, it relaxes the boundary conditions of zero stress, which will cause a certain error in the result. Therefore, if calculation accuracy is required, the part of the reflected wave must be removed from the scattering caused by the large arc [11]. We introduce dimensionless residual stress to describe the accuracy of the series solution and guide programming calculations. Substitute the calculated coefficients back into the equation and use the condition that the boundary radial stress is zero to test. We have the following definitions.

Residual stress of the outer lining surface:

$$\tau_{z\rho}^{b} = \left| \frac{\left(\tau_{z\rho 2}^{(S2)} + \tau_{z\rho 2}^{(S3)} + \tau_{z\rho 2}^{(S4)} - \tau_{z\rho 2}^{(\Gamma b)} - \tau_{z\rho 2}^{(\Gamma a)}\right)}{\left(ik_1\mu_1 W_0\right)} \right|_{|z_2|=b}. \tag{20}$$

Residual stress of the inner lining surface:

$$\tau_{z\rho}^{a} = \left| \frac{\left(\tau_{z\rho 2}^{(\Gamma b)} + \tau_{z\rho 2}^{(\Gamma a)}\right)}{\left(ik_1\mu_1 W_0\right)} \right|_{|z_2|=a}. \tag{21}$$

Next, we use model degradation to compare existing research results to verify the feasibility of this method. When the medium parameter is set to $\mu^* = k^* = \rho^* = 1$ and $\mu^\# = \rho^\# = 1$, the parameters of Layer A, Layer B, and Region C are the same. The three are merged into the same area. At this time, the problem is reduced to a half-space problem of a single soil layer. There is a circular hole with a radius of $a = 1$. Figure 6(a) shows the *DSCF* around the circular hole, which is basically consistent with the results in [10]. Figure 6(b) shows the *DSCF* of the inner boundary of the lining under the action of incident waves with three frequencies of $k_1 a = 0.1, 1.0, 2.0$, which are basically consistent with the results in [14].

The Bessel function with good convergence is used. As long as the number of series items is appropriate, the maximum of residual radial stress can be sufficiently small (such as less than 1%) to meet the accuracy requirements. This conclusion also applies to other issues [30]. Figures 6(c) and 6(d) are the residual radial stress plots of the inner and outer boundaries of the lining, respectively. It can be seen that when both m and n are set to 12, the residual radial stress is around $10^{-5} \sim 10^{-6}$.

In the research of this article, it can be ensured that the magnitude of the stress residual is around 10^{-6}; when $k_1 a \le 0.5$, take the number of truncated items $m = n \ge 8$, and when $0.5 \le k_1 a \le 2.4$, take the number of truncated items $m = n = 14$. This can provide accuracy guarantee for the research of this article.

Through the above verification, it is proved that the analysis method of SH wave scattering in composite strata in this paper is also applicable to half-space problems, and the conclusions of the two can be mutually corroborated. We adopt the large-arc assumption and properly select the truncation terms of the equation, which can meet the accuracy requirements for solving such problems and lay the foundation for the discussion of the numerical examples in this paper.

4. Numerical Examples and Analysis

In addition to structural damage, dynamic stress concentration is an important factor that causes tunnel damage in earthquakes. The ratio of the actual stress around the tunnel to the maximum incident stress is usually defined as the *DSCF*. The maximum value is expressed as $DSCF_{\max}$. The corresponding dynamic stress concentration factor in this study is

$$\begin{aligned} DSCF &= \left| \frac{\left(\tau_{z\varphi 2}^{(\Gamma b)} + \tau_{z\varphi 2}^{(\Gamma a)}\right)}{\left(ik_1\mu_1 W_0\right)} \right|_{|z_2|=r_2}, \\ \tau_{z\varphi 2}^{(\Gamma b)} &= \frac{ik_3\mu_3}{2} \sum_{n=-\infty}^{n=+\infty} C_{En} \left\{ H_{n-1}^{(2)}\left[k_3 \left(z_2\bar{z}_2\right)^{1/2}\right] \right. \\ &\quad \left. + H_{n+1}^{(1)}\left[k_3 \left(z_2\bar{z}_2\right)^{1/2}\right] \right\} \left(\frac{z_2}{\bar{z}_2}\right)^{n/2}, \\ \tau_{z\varphi\left(z_2,\bar{z}_2\right)}^{(\Gamma a)} &= \frac{ik_3\mu_3}{2} \sum_{n=-\infty}^{n=+\infty} C_{Fn} \left\{ H_{n-1}^{(1)}\left[k_3 \left(z_2\bar{z}_2\right)^{1/2}\right] \right. \\ &\quad \left. + H_{n+1}^{(1)}\left[k_3 \left(z_2\bar{z}_2\right)^{1/2}\right] \right\} \left(\frac{z_2}{\bar{z}_2}\right)^{n/2}. \end{aligned} \tag{22}$$

In this paper, we assume that the inner diameter of the circular lining $a = 1$ and the buried depth $h_1 = 1.5a$; SH waves are incident vertically ($\alpha_0 = 90^\circ$). Figure 7 shows the *DSCF* of the C30 concrete lining inner and outer surfaces when the SH wave is incident perpendicularly from the basalt layer to the sandstone layer in geological Condition A. At this time, the composite stratum is "soft-over-hard" with "flexible lining." First, the relationship between *DSCF* and the incident wave frequency is analyzed. The two figures show that when $k_1 a = 0.1$, that is, when a low-frequency wave is incident, $DSCF_{\max}$ appears at approximately 200° and 340°. With the increase in the incident frequency, when $k_1 a = 1.0$, that is, for an intermediate-frequency incident waves, the overall magnitude of *DSCF* significantly increases. The positions of $DSCF_{\max}$ change, appearing at 20° and 160°. When $k_1 a = 2.0$ (high-frequency incidence), the distribution shape becomes more complicated, but the overall value of *DSCF* is smaller, and the positions of $DSCF_{\max}$ appear at about 0° and 180°. Under Condition A, as $k_1 a$ increases, *DSCF* of C30 concrete lining gradually changes from small to large and then to small again. The dynamic stress concentration of the lining is most obvious

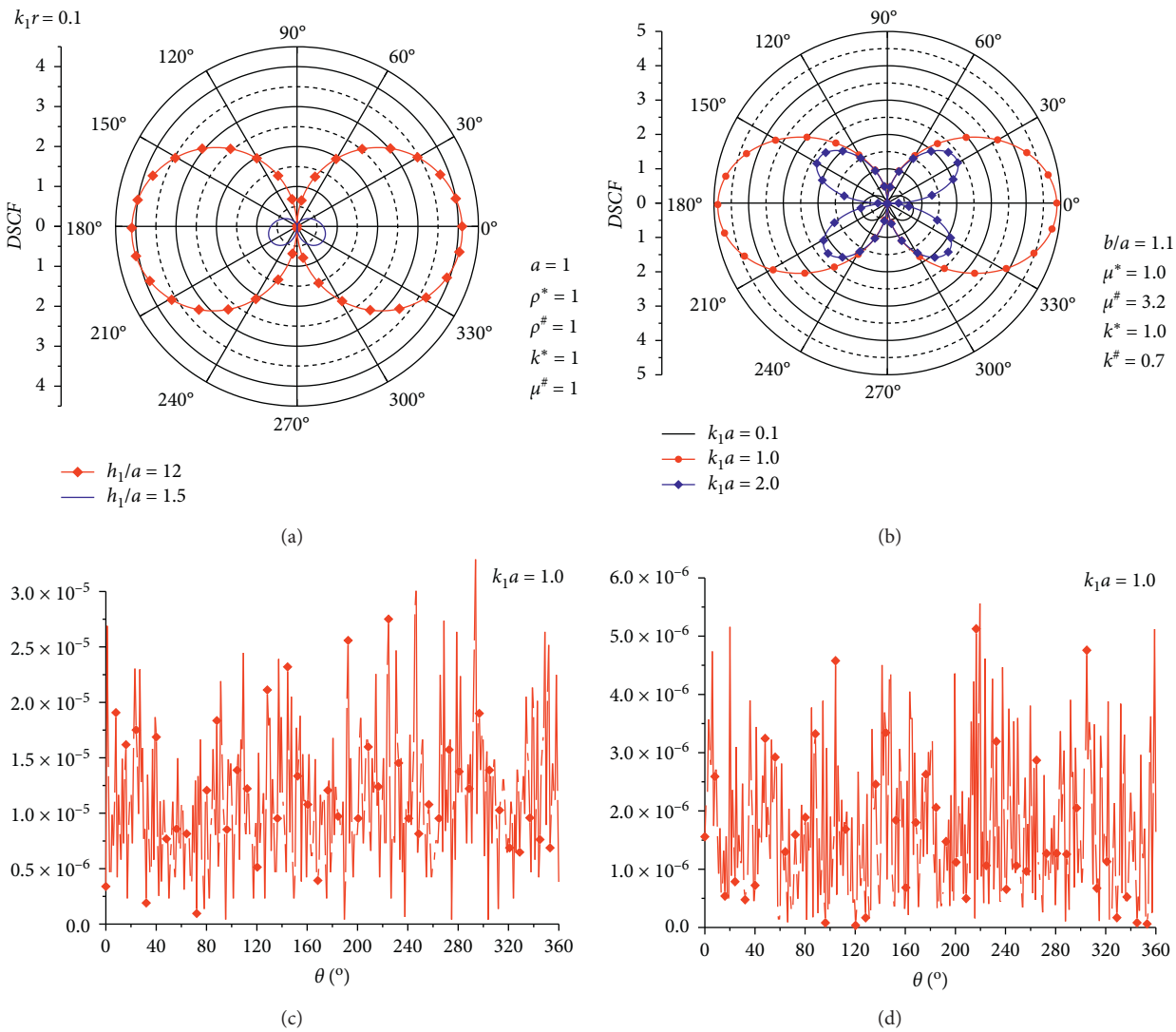

Figure 6: The verification calculation when degenerated into the half-space problem. (a) *DSCF* along the edge of a cavity in half-space. (b) *DSCF* along the inner surface of a circular lining in half-space. (c) Residual radial stress on the inner surfaces of a circular lining in half-space. (d) Residual radial stress on the outer surfaces of a circular lining in half-space.

under the action of intermediate frequency incident waves. Looking at the distribution of *DSCF* on the lining, the overall value of *DSCF* on the inner surface in Figure 7(a) is larger than the *DSCF* on the outer surface in Figure 7(b), indicating that the damage of the inner surface at this time is something we need to care about. Finally, we analyze the impact of lining thickness on *DSCF*. For the inner surface of C30 concrete lining, *DSCF* gradually becomes larger as the lining thickness increases, while *DSCF* on the outer surface becomes smaller as the lining thickness increases. In the composite stratum, the distribution of *DSCF* of the "flexible lining" is more complicated than that in the half space. It is not that the thicker the lining is, the more beneficial it is to reduce *DSCF*.

Figure 8 shows the *DSCF* of the Q345 steel lining in Condition A. At this time, the composite stratum is "soft-over-hard" with "rigid lining." Consistent with the law in Figure 7, the *DSCF* of Q345 steel lining increases with k_1a, and *DSCF* changes from small to large and then to small again, which is significant to the dynamic response of the intermediate frequency incident wave. Compared with Figure 7, in Figure 8, because "flexible lining" is easier to absorb energy than "rigid lining," when the lining thickness ratio $(b/a) \geq 1.2$, the overall value of *DSCF* of Q345 steel lining is smaller than that of C30 concrete lining. However, when $(b/a) = 1.05$, when the lining is thinner, this phenomenon is not obvious. The values of *DSCF* of the inner surface and outer surface of the Q345 steel lining are relatively close, and both become smaller as the thickness of the lining increases. Therefore, under this geological combination, the thickness of the Q345 steel lining is appropriately increased, which is beneficial to reduce the *DSCF* of the lining.

The difference of the site is an important factor affecting the characteristics of seismic wave propagation in different frequency bands. From the perspective of engineering

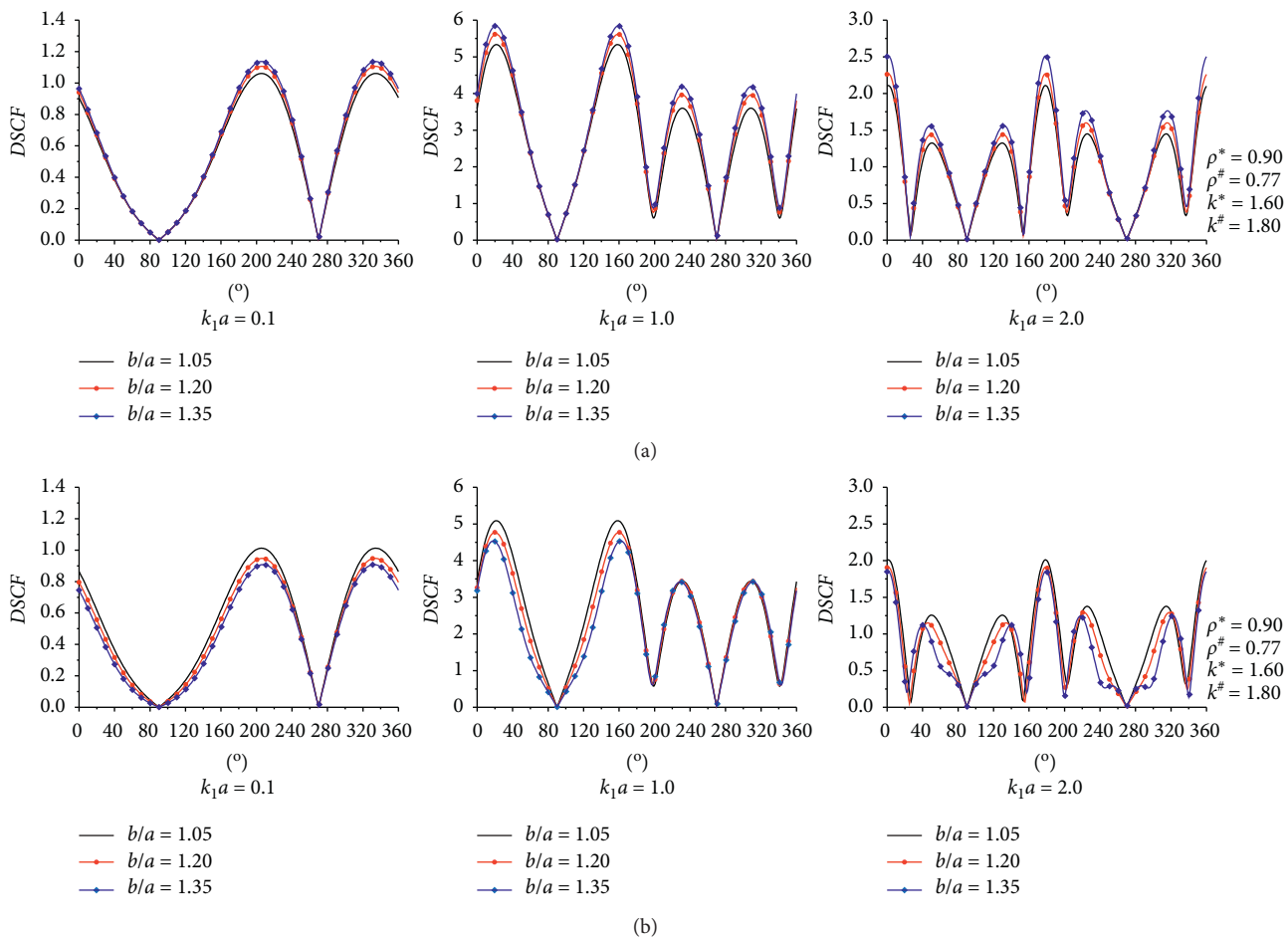

Figure 7: $DSCF$ of linings composed of grade C30 concrete for geological condition A. (a) Condition A-C30: inner surface. (b) Condition A-C30: outer surface.

application, it is necessary to conduct a comprehensive analysis combining the specific material parameters of the stratum and the lining to find the most sensitive frequency of the lining to the incident wave dynamic response. We divide the frequency of the SH wave from $k_1a \approx 0.1$ to $k_1a \approx 2.5$ into 99 segments and 100 points and extract $DSCF_{\max}$ on the inner surface of the lining each time. Figure 9 shows the change of $DSCF_{\max}$ with k_1a in the case of Condition A. There are four obvious peaks in $DSCF_{\max}$ of the lining in the two figures, but the peak is the largest at $k_1a \approx 0.35$, and thereafter it shows a trend of decreasing oscillation. This shows that, in the "soft-over-hard" type of composite stratum, the impact of the mid-low frequency incident wave on the $DSCF$ is relatively large. In Figure 9(a), we can see the same rule as that in Figure 7(a). Increasing the thickness of the C30 concrete lining will increase $DSCF_{\max}$ of the inner surface of the lining. Figure 9(b) reflects the same rule as that in Figure 8(a). Increasing the thickness of the Q345 steel lining can reduce $DSCF_{\max}$ of the inner surface of the lining. Obtaining this rule is meaningful for us to use different materials as the lining of tunnels or pipelines for engineering design, and it can help us make reasonable judgments on the thickness of the lining.

Figure 10 shows the $DSCF$ of the C30 concrete lining in geological Condition B. The composite stratum is "hard-over-soft" with "flexible lining." Compared with Figure 7,$DSCF$ in Figure 10 is considerably reduced on the whole. As the surface soil layer hardens, the $DSCF$ around the lining decreases overall. The preliminary judgment is that because the SH wave from the lower soft soil layer is shielded by the surface hard soil layer, the energy of the wave propagating into the sandstone layer is reduced, which reduces the $DSCF$ around the lining. The high-frequency incident wave has a greater influence on the dynamic stress concentration phenomenon of the lining. As in the case of Condition A, the overall value of $DSCF$ of the inner surface of the C30 concrete lining is greater than that of the inner surface. The $DSCF$ of the inner surface gradually becomes larger as the thickness of the lining becomes larger, and the $DSCF$ of the outer surface gradually becomes smaller as the thickness of the lining becomes larger.

Figure 11 shows the $DSCF$ of the Q345 steel lining in Condition B. At this time, the composite stratum is "hard-over-soft" with "rigid lining." The hard surface soil layer also greatly reduces the $DSCF$ around the lining. The $DSCF$ of the inner surface gradually becomes larger as the thickness of the lining becomes larger, and k_1a of the outer surface gradually becomes smaller as the thickness of the lining becomes larger. When the lining thickness ratio $(b/a) \geq 1.2$,

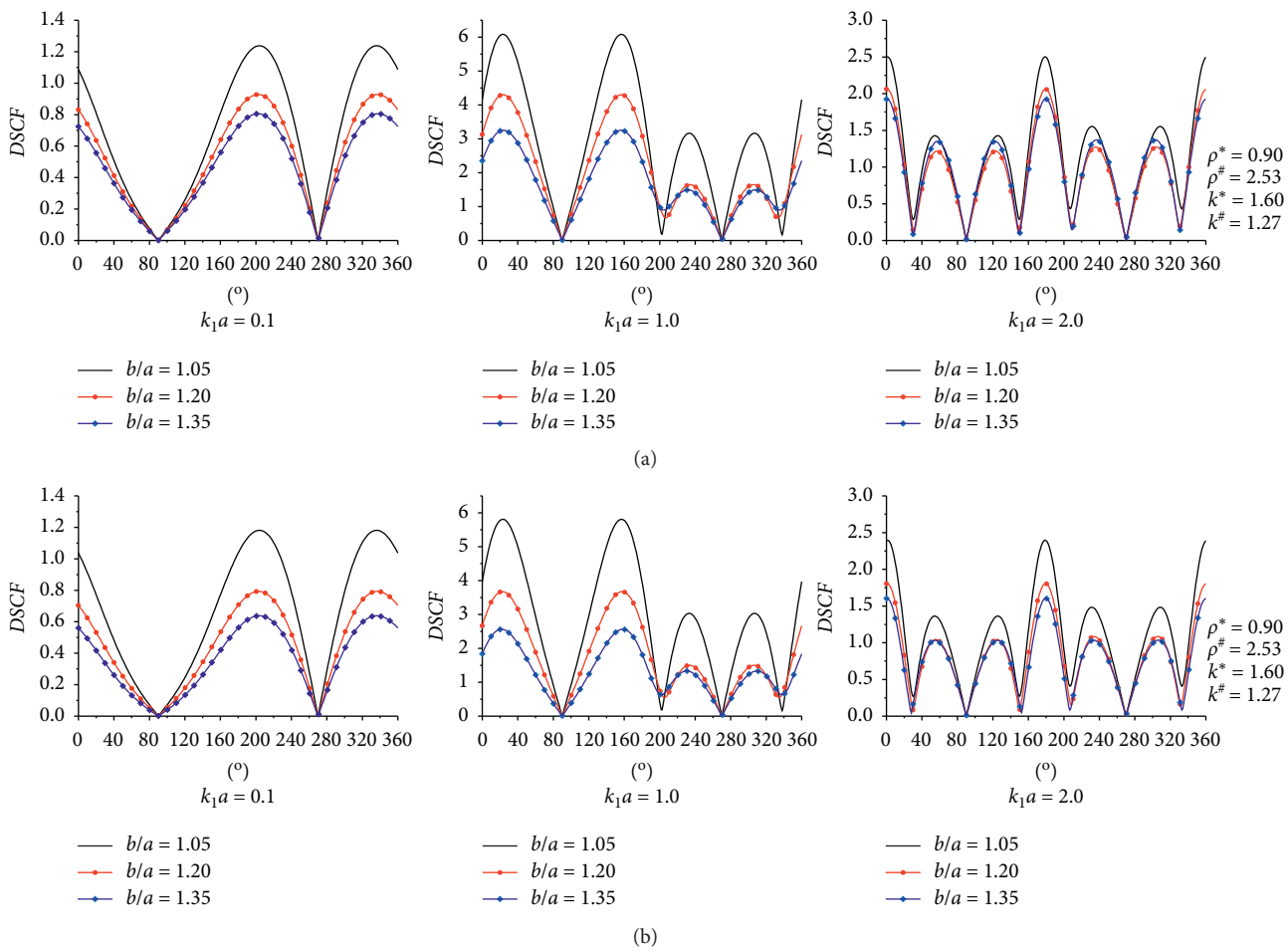

Figure 8: $DSCF$ of linings composed of grade Q345 steel for geological Condition A. (a) Condition A-Q345: inner surface. (b) Condition A-Q345: outer surface.

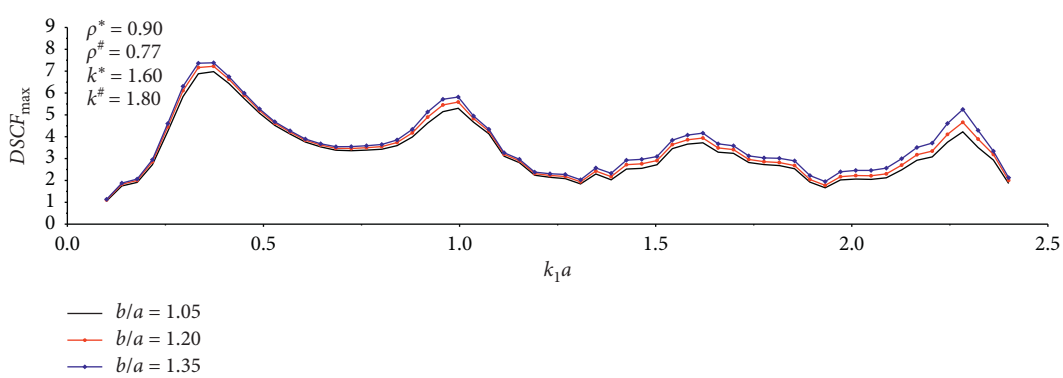

(a)

Figure 9: Continued.

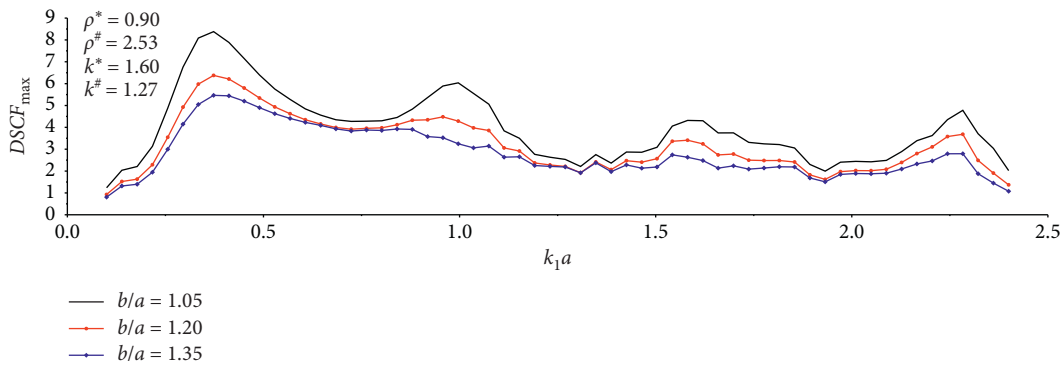

(b)

Figure 9: Variation of $DSCF_{max}$ with k_1a on the inner surface of linings for geological Condition A. (a) Condition A-C30: inner surface. (b) Condition A-Q345: inner surface.

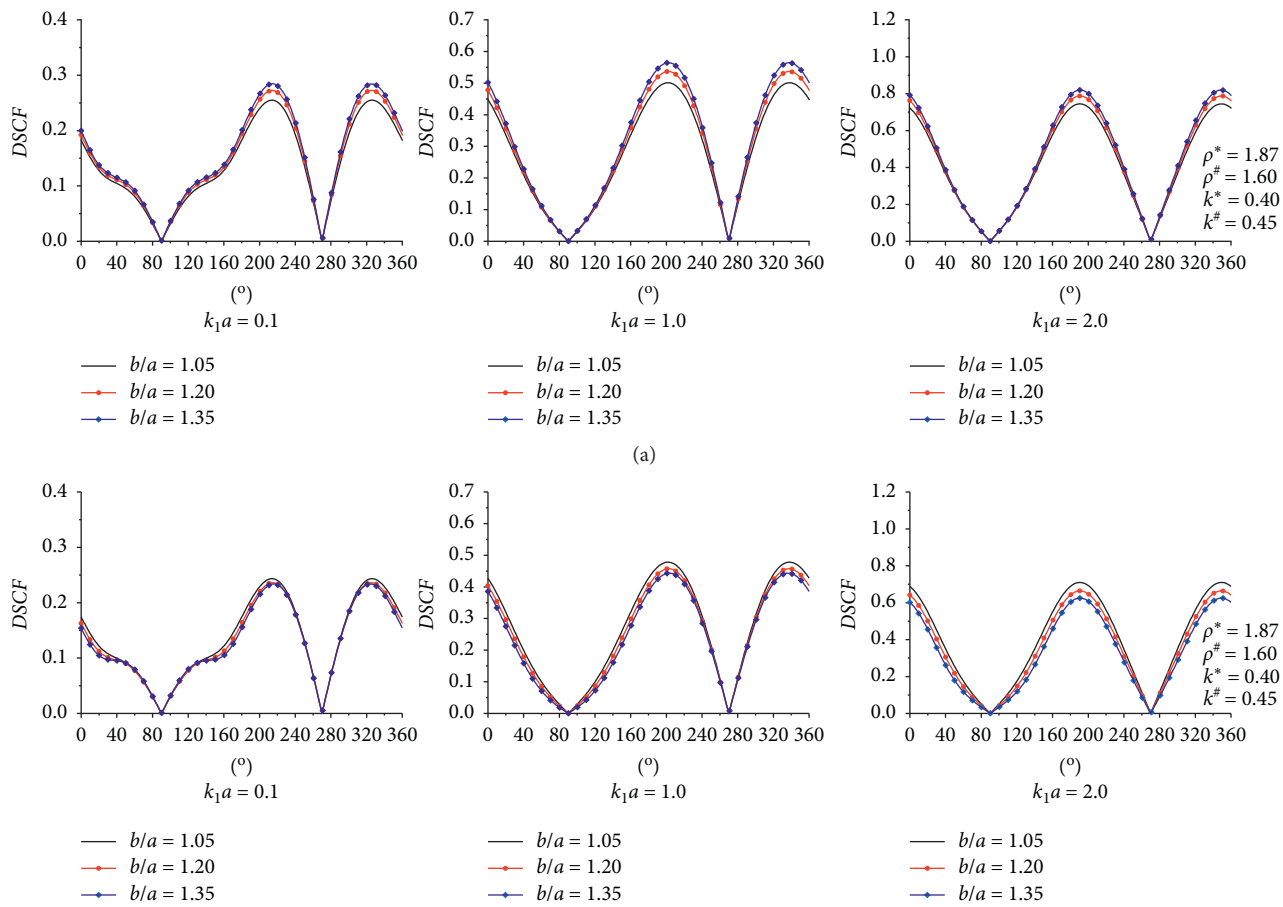

(a)

(b)

Figure 10: $DSCF$ of linings composed of grade C30 concrete for geological Condition B. (a) Condition B-C30: inner surface. (b) Condition B-C30: outer surface.

the overall value of $DSCF$ of the Q345 steel lining is smaller than the $DSCF$ of the C30 concrete lining, and the $DSCF$ of the outer surface is smaller than the $DSCF$ of the inner surface. When $(b/a) = 1.05$, and when the lining is thinner, the two values of $DSCF$ are relatively close. It is then well founded that appropriately increasing the thickness of the Q345 steel lining is also beneficial for reducing the $DSCF$ of the lining.

Figure 12 shows the change of $DSCF_{max}$ with k_1a in the case of Condition B. Compared with Figure 9, the overall value of $DSCF_{max}$ in Figure 12 has been significantly reduced. This is the typical difference between the "hard-over-

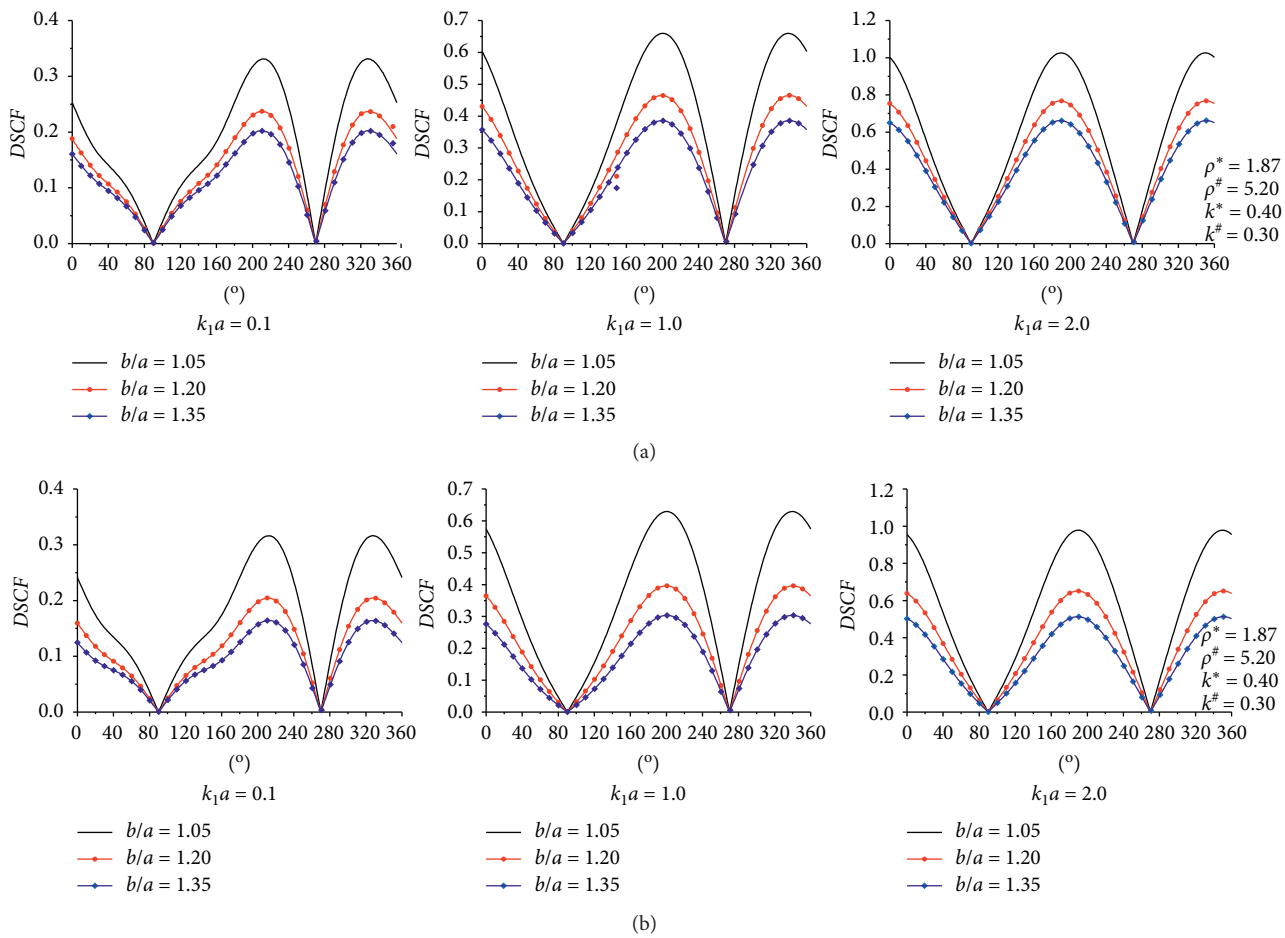

Figure 11: $DSCF$ of linings composed of grade Q345 steel for geological Condition B. (a) Condition B-Q345: inner surface. (b) Condition B-Q345: outer surface.

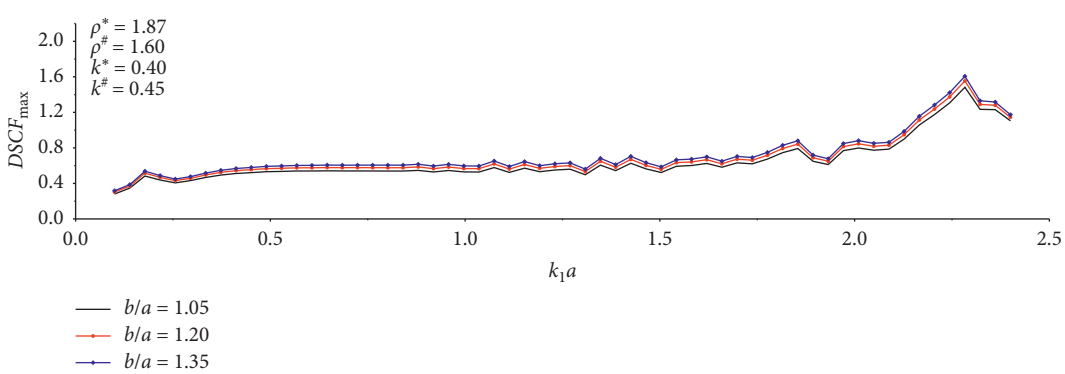

(a)

Figure 12: Continued.

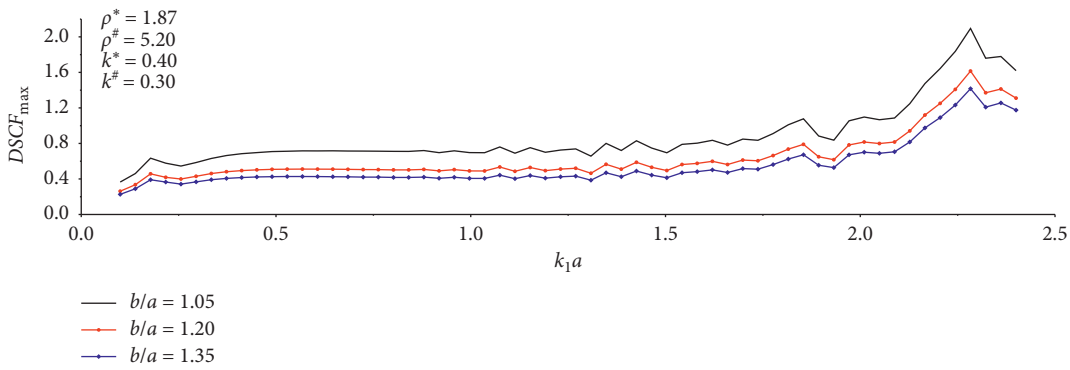

(b)

Figure 12: Variation of $DSCF_{max}$ with k_1a on the inner surface of linings for geological Condition B. (a) Condition B-C30: inner surface. (b). Condition B-Q345: inner surface.

soft" composite stratum and the "soft-over-hard" composite stratum. The change of $DSCF_{max}$ in geological Condition A is close to the problem in half-space, and both are more sensitive to SH waves of middle and low frequency. The dynamic response of the lining is greater when the frequency of the incident wave is higher in the case of Condition B. $DSCF_{max}$ becomes close to the maximum when $k_1a = 2.3$, not in the mid-low frequency. This phenomenon indicates that the sensitive frequency of the dynamic response is jointly affected by the media parameters of the soil layers, which also proves once again that it is meaningful to study the scattering of SH waves by linings in composite strata. On the basis of studying the half-space problem, we have further enriched our understanding of the SH-wave scattering problem under the influence of various factors such as different soil layers and linings of different materials.

5. Conclusions

(1) The $DSCF$ of the lining will be enlarged by the soft surface soil layer and reduced by the hard surface soil layer. When the lining thickness ratio $(b/a) \geq 1.2$, "flexible lining" is easier to absorb energy than "rigid lining," and $DSCF$ is larger. When the lining thickness is relatively small, this phenomenon is not obvious.

(2) Compared with the problem in half-space, the combination of parameters in composite formation is more complicated. The "soft-over-hard" composite strata are more sensitive to incident waves at low and intermediate frequencies, while the "hard-over-soft" composite strata are more sensitive to high-frequency incident waves.

(3) For Q345 steel lining, increasing the thickness of the lining is effective in reducing the $DSCF$. But, for C30 concrete, increasing the thickness of the lining reduces the $DSCF$ of the outer lining surface while increasing the $DSCF$ of the inner lining surface. This effect should be considered in engineering, and differentiated strengthening measures should be taken for the inner and outer surfaces.

Data Availability

The data used to support the findings of this study are included within the article.

Conflicts of Interest

The authors declare that there are no conflicts of interest regarding the publication of this paper.

Acknowledgments

This work was supported by the Fundamental Research Funds for Central Universities (3072020CF0206).References

[1] Y. M. A. Hashash, J. J. Hook, B. Schmidt, and J. Chiang Yao, "Seismic design and analysis of underground structures," *Tunnelling and Underground Space Technology*, vol. 16, no. 4, pp. 247–293, 2001.

[2] X.-Q. Fang, H.-X. Jin, and B.-L. Wang, "Dynamic interaction of two circular lined tunnels with imperfect interfaces under cylindrical P-waves," *International Journal of Rock Mechanics and Mining Sciences*, vol. 79, pp. 172–182, 2015.

[3] X.-Q. Fang, H.-C. Huang, and J.-X. Liu, "Predicting the crack opening displacements of a partially debonded pipeline in rock mass under P waves," *Fatigue & Fracture of Engineering Materials & Structures*, vol. 39, no. 7, pp. 886–895, 2016.

[4] X.-Q. Fang, T.-F. Zhang, B.-L. Li, and R.-J. Yuan, "Elastic-slip interface effect on dynamic stress around twin tunnels in soil medium subjected to blast waves," *Computers and Geotechnics*, vol. 119, p. 103301, 2020.

[5] İ. Coşkun and D. Dolmaseven, "Dynamic response of a circular tunnel in an elastic half space," *Journal of Engineering*, vol. 2017, Article ID 6145375, 2017.

[6] D. H. Carlson, C. C. Plummer, and D. McGeary, *Physical Geology*, McGraw-Hill, New York, NY, USA, 2006.

[7] J. Steingrimsson, E. Grøv, and B. Nilsen, "The significance of mixed-face conditions for TBM performance," *World Tunnelling*, vol. 15, no. 9, pp. 435–441, 2002.

[8] Á. Tóth, Q. Gong, and J. Zhao, "Case studies of TBM tunneling performance in rock-soil interface mixed ground," *Tunnelling and Underground Space Technology*, vol. 38, pp. 140–150, 2013.

[9] D. Liu, B. Gai, and G. Tao, "Applications of the method of complex functions to dynamic stress concentrations," *Wave Motion*, vol. 4, no. 3, pp. 293–304, 1982.

[10] H. Lin and D. Liu, "Scattering of SH-wave around a circular cavity in half space," *Earthquake Engineering and Engineering Vibration*, vol. 22, pp. 9–16, 2002.

[11] C. A. Davis, V. W. Lee, and J. P. Bardet, "Transverse response of underground cavities and pipes to incident SV waves," *Earthquake Engineering & Structural Dynamics*, vol. 30, no. 3, pp. 383–410, 2001.

[12] J. W. Liang, H. Zhang, and V. W. Lee, "An analytical solution for dynamic stress concentration of underground cavities under incident plane P waves," *Chinese Jounal of Geotechnical Engineering*, vol. 26, no. 6, pp. 815–819, 2004.

[13] H. Qi and J. Yang, "Dynamic analysis for circular inclusions of arbitrary positions near interfacial crack impacted by SH-wave in half-space," *European Journal of Mechanics-A/Solids*, vol. 36, pp. 18–24, 2012.

[14] Q. Hui, Y. Wang, and D.-K. Liu, "Dynamic analysis of shallow-embedded lining structure by incident SH-wave," *Earthquake Engineering and Engineering Vibration*, vol. 3, 2003.

[15] K. Yoshimoto, S. Takemura, and M. Kobayashi, "Application of scattering theory to P-wave amplitude fluctuations in the crust," *Earth Planets & Space*, vol. 67, no. 1, pp. 1–15, 2015.

[16] H. P. Brandow and V. Lee, "Scattering and diffraction of plane P-waves in a 2-D elastic half-space II: shallow arbitrary shaped canyon," *Earthquake Engineering and Engineering Vibration*, vol. 16, no. 3, pp. 459–485, 2017.

[17] Q. Liu, M. Zhao, and Z. Liu, "Wave function expansion method for the scattering of SH waves by two symmetrical circular cavities in two bonded exponentially graded half spaces," *Engineering Analysis with Boundary Elements*, vol. 106, pp. 389–396, 2019.

[18] Z. Yang, Y. Song, X. Li, G. Jiang, and Y. Yang, "Scattering of plane SH waves by an isosceles trapezoidal hill," *Wave Motion*, vol. 92, p. 102415, 2020.

[19] M. Tao, H. T. Zhao, Z. W. Li, and J. B. Zhu, "Analytical and numerical study of a circular cavity subjected to plane and cylindrical P-wave scattering," *Tunnelling and Underground Space Technology*, vol. 95, p. 103143, 2020.

[20] Z. Ba and X. Gao, "Soil-Structure interaction in transversely isotropic layered media subjected to incident plane SH waves," *Shock and Vibration*, vol. 2017, Article ID 2834274, 13 pages, 2017.

[21] J. Liang, Z. Liu, L. Huang, and G. Yang, "The indirect boundary integral equation method for the broadband scattering of plane P, SV and Rayleigh waves by a hill topography," *Engineering Analysis with Boundary Elements*, vol. 98, pp. 184–202, 2019.

[22] Z. Ba and X. Yin, "Wave scattering of complex local site in a layered half-space by using a multidomain IBEM: incident plane SH waves," *Geophysical Journal International*, vol. 205, no. 3, pp. 1382–1405, 2016.

[23] Z. Ba, Y. Wang, J. Liang, and V. W. Lee, "Wave scattering of plane P, SV, and SH waves by a 3D alluvial basin in a multilayered half-space," *Bulletin of the Seismological Society of America*, vol. 110, no. 2, pp. 576–595, 2020.

[24] Z. Ba, E. Zhang, J. Liang, Y. Lu, and M. Wu, "Two-dimensional scattering of plane waves by irregularities in a multilayered transversely isotropic saturated half-space," *Engineering Analysis with Boundary Elements*, vol. 118, pp. 169–187, 2020.

[25] H. Xu, T. Li, J. Xu, and Y. Wang, "Dynamic response of underground circular lining tunnels subjected to incident P waves," *Mathematical Problems in Engineering*, vol. 2014, Article ID 297424, 2014.

[26] L. Jian-wen, "Scattering of plane P waves by circular-arc layered alluvial valleys: an analytical solution," *Acta Seismologica Sinica*, vol. 14, no. 2, pp. 176–195, 2001.

[27] V. W. Lee and W.-Y. Liu, "Two-dimensional scattering and diffraction of P- and SV-waves around a semi-circular canyon in an elastic half-space: an analytic solution via a stress-free wave function," *Soil Dynamics and Earthquake Engineering*, vol. 63, pp. 110–119, 2014.

[28] V. W. Lee, W. Y. Liu, M. D. Trifunac, and N. Orbović, "Scattering and diffraction of earthquake motions in irregular elastic layers, I: love and SH waves," *Soil Dynamics and Earthquake Engineering*, vol. 66, pp. 125–134, 2014.

[29] D.-H. Tsaur and K.-H. Chang, "Exact solution to scattering of SH waves by an elliptic-arc canyon in the corner of an elastic quarter space," *Soil Dynamics and Earthquake Engineering*, vol. 110, pp. 137–140, 2018.

[30] X.-M. Yuan, "Effect of a circular underground inclusion on surface motion under incident plane SH waves," *Acta Geophysica Sinica*, vol. 39, no. 3, pp. 373–381, 1996.